Journal of Alloys and Compounds 508 (2010) 278–291

Contents lists available at ScienceDirect

Journal of Alloys and Compounds

journal homepage: www.elsevier.com/locate/jallcom

Influence of tungsten on the emission features of Nd^{3+}, Sm^{3+} and Eu^{3+} ions in ZnF_2–WO_3–TeO_2 glasses

Y. Gandhi[a], I.V. Kityk[b], M.G. Brik[c], P. Raghava Rao[a], N. Veeraiah[a,*]

[a] Department of Physics, Acharya Nagarjuna University–Nuzvid Campus, Nuzvid 521 201, A.P., India
[b] Electrical Engineering Department, Technical University of Czestochowa, Aleja, Armii, Krajowej 17/19, PL-42-201 Czestochowa, Poland
[c] Institute of Physics, University of Tartu, Riia 142, Tartu 51014, Estonia

ARTICLE INFO

Article history:
Received 29 July 2010
Received in revised form 11 August 2010
Accepted 27 August 2010

Keywords:
TeO_2 glasses
Tungsten ions
Rare earth ions
Spectroscopic properties

ABSTRACT

The glasses of the composition $(45-x)ZnF_2$–xWO_3–$49TeO_2$:$1.0Nd_2O_3/Sm_2O_3/Eu_2O_3$ with x varying from 5 to 20 mol% were synthesized. Optical absorption, fluorescence spectra (in the spectral range 400–2300 nm) and also fluorescence decay were studied at ambient temperature. The Judd–Ofelt theory analysis was applied to characterize the absorption and luminescence spectra of Ln^{3+} ions in these glasses. Following the luminescence spectra, various radiative properties like transition probability A, branching ratio β and the radiative life time τ for $^4F_{3/2} \rightarrow {}^4I_{11/2}$, $^4G_{5/2} \rightarrow {}^6H_{7/2}$, $^5D_0 \rightarrow {}^7F_2$ emission levels respectively for Nd^{3+}, Sm^{3+} and Eu^{3+} doped glasses of these glasses have been evaluated. The variations observed in these parameters were discussed following of varying co-ordinations (tetrahedral and octahedral positions) and the valence states of tungsten ions in the glass network. A significant enhancement in the intensities of $^4F_{3/2} \rightarrow {}^4I_{11/2}$ (Nd^{3+}), $^4G_{5/2} \rightarrow {}^6H_{7/2}$ (Sm^{3+}) and $^5D_0 \rightarrow {}^7F_2$ (Eu^{3+}) emission lines has been observed with increase of WO_3 content; this is attributed to the increase in the concentration W^{5+} ions in the glass network that acts as modifiers. The quantitative analysis of these results (with the aid of the data on ESR, IR and Raman spectral studies) has indicated that the glasses mixed with around 15 mol% of WO_3 have the optimum concentration for yielding the highest quantum efficiency with low phonon losses for the above-mentioned principal transitions.

1. Introduction

Tellurium oxide based glasses are well known due to their high density, high transparency in the mid infrared region (~5.0–11.0 μm), high linear and non-linear refractive index, good stability against moisture [1–5]. In view of such qualities, these glasses find potential applications as IR domes, optical fibers, modulators, non-linear optical devices and infrared laser windows. These are also considered as good glasses for hosting rare earth ions since they provide a low phonon energy (~750 nm, lower than geramanate, phosphate and silicate glasses) environment that minimizes non-radiative losses [6–8]. The presence of tungsten ions in these glasses, further, makes them suitable for optoelectronic devices since they exhibit photochromism and electrochromism properties. Tungsten ions are expected to have profound influence on luminescence characteristics of rare earth ions in tellurite glasses, for the simple reason that these ions exist in different valence states viz., W^{6+}, W^{5+} and also in W^{4+} as per the following thermo reversible disproportionate reaction:

$$W^{5+} + W^{6+} \leftrightarrow W^{4+} + W^{6+}$$

regardless of the oxidation state of the tungsten ion in the starting glass batch [10–13,9].

Among these, W^{6+} ions participate in the glass network with different structural units like WO_4 (T_d) and WO_6 (O_h). The WO_4 units form the linkages of the type Te–O–W with TeO_4 and TeO_3 structural units in the glass network since the electronegativities (2.1 for Te ion and 2.0 for W^{6+} ion) are very close to each other. On the other hand W^{5+} ($5d^1$) ions forming the complexes of $W^{5+}O_3^-$, act as modifiers and induce structural disorder in the tellurite network by transforming TeO_4 to TeO_{3+1} structural units in the glass network. Hence, the varying concentration of WO_3 in the glass network results varying environment of luminescent ions present in the tellurite glass network. As a consequence, interesting changes in the luminescent characteristics of lasing ions is expected.

The addition of ZnF_2 to tellurite glass matrix is anticipated to contribute to the chemical inertness of the glasses since there is a possibility for the formation of covalent bonding between tellurite and zinc ions through non-bridging oxygens (Te–O–Zn) [14,15].

The study on absorption and emission characteristics of Nd^{3+} ($4f^3$) ion has been subject of extensive investigation in a number of

* Corresponding author. Tel.: +91 8656 235551; fax: +91 8656 235551.
E-mail address: nvr8@rediffmail.com (N. Veeraiah).

0925-8388/$ – see front matter © 2010 Elsevier B.V. All rights reserved.
doi:10.1016/j.jallcom.2010.08.137

crystalline and glass materials because of its prospective applications in NIR laser technology [16–20]. The transition $^4I_{9/2} \rightarrow {}^2P_{1/2}$ (around 430 nm) in the absorption spectra is a characteristic of coordination of this ion. Generally this band is desirable in the construction of compact and efficient laser source pumped by diode laser. The impact of changing environment in the glass network due to the variation in the concentration of the tungsten ions is expected to very high on this transition.

Samarium containing glasses are known to have an unusual elastic behaviour due to valance instability [21]. This ion exists in trivalent and divalent states but between these two states, Sm^{3+} ($4f^5$) is found to be more stable. Samarium exhibits promising characteristics for spectral hole burning studies [22,23]. The decay of exited states in Sm^{3+} involves different mechanisms depending on the matrix. Earlier studies on optical absorption, fluorescence and lifetime measurements of Sm^{3+} ions in oxyfluoroborate and oxide glasses have indicated the quenching of the fluorescence of $^4G_{5/2}$ level [24,25]; this is attributed to quadrupole–quadrupole interaction among the samarium ions. Similarly, a number of earlier studies on spectroscopic properties of Sm^{3+} ions in different glass matrices have revealed that the fluorescence yield of this rare earth ion is strongly dependent on its environment inside the glass network [26–31].

Europium ion, another interesting rare earth ion, has got variable valency states, Eu^{3+} and Eu^{2+}. Eu^{3+} ($4f^6$ ion) is quite stable even at high temperatures in crystalline and glassy host matrices. The transitions, $^7F_0 \rightarrow {}^5D_2$ in the absorption spectrum and $^5D_0 \rightarrow {}^7F_2$ in the emission spectrum of Eu^{3+} are reported to be hypersensitive; the integrated emission intensity ratio of $^5D_0 \rightarrow {}^7F_2$ (red) and $^5D_0 \rightarrow {}^7F_1$ (orange) transitions (R/O ratio) is strongly influenced by site asymmetry and covalency of the bonds with the ligand anion [32,33]. The effect of surrounding ions on the luminescence of europium in glass has been reported in several works [34–36] which clearly indicated that the relative intensities of the Eu^{3+} emission peaks depend strongly on the variations in the glass network at the vicinity of this ion. Eu^{3+} ion has the additional feature of interest; phonon side band studies can give information about the electron–phonon coupling strength with the host lattice and also throw light whether, non-radiative or radiative decay is favoured.

The thorough literature survey on TeO_2 glasses as laser host materials, indicates that though some considerable number of studies on WO_3–TeO_2 glasses are available [37,38], still there is a lot of scope to investigate the influence of the tungsten ions on the emission characteristics of rare earth ions. The objective of the present investigation is to study the fluorescence features of three different rare earth ions viz., Nd^{3+}, Eu^{3+} and Sm^{3+} ions in the visible and infrared regions in ZnF_2–WO_3–TeO_2 glass system with the gradual increase of WO_3 content in the glass network at the expense of ZnF_2. The results of ESR, IR and Raman spectral studies have also been used to have a comprehensive pre-knowledge over the structural changes in the glass network due to the variations in the concentrations of WO_3 at the vicinity of rare earth ions which influence the luminescence efficiency.

2. Experimental

Within the glass forming region (Fig. 1) of ZnF_2–WO_3–TeO_2 glass system, a particular composition $(50-x)ZnF_2$–xWO_3–$49TeO_2$:$1Ln_2O_3$ (with x ranging from 5 to 20) is chosen for the present study. The details of the composition are:

LnW_5: $45ZnF_2$–$5WO_3$–$49TeO_2$: $1Ln_2O_3$

LnW_{10}: $40ZnF_2$–$10WO_3$–$49TeO_2$: $1Ln_2O_3$

LnW_{15}: $35ZnF_2$–$15WO_3$–$49TeO_2$: $1Ln_2O_3$

LnW_{20}: $30ZnF_2$–$20WO_3$–$49TeO_2$: $1Ln_2O_3$

where Ln = Nd, Sm and Eu.

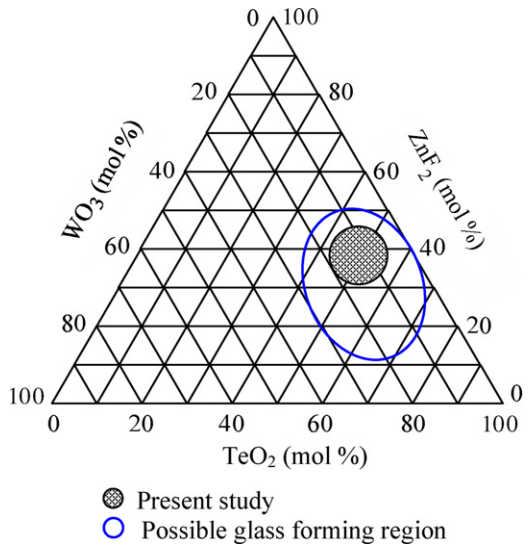

Fig. 1. Approximate glass forming region of ZnF_2–WO_3–TeO_2 glass system.

Appropriate amounts (all in mol%) of reagent grades of ZnF_2, WO_3, TeO_2, Nd_2O_3, Sm_2O_3 and Eu_2O_3 (METALL, China, 4N pure) powders were thoroughly mixed in an agate mortar and melted in a thick-walled platinum crucible in the temperature range 650–700 °C in an automatic temperature controlled furnace for about 1 h until a bubble free transparent liquid was formed. The resultant melt was then poured in a brass mould and subsequently annealed from 250 °C with a cooling rate of 1 °C/min. The samples used for optical absorption, luminescence spectra studies were prepared by suitable grinding and optical polishing to the dimensions of 1 cm × 1 cm × 0.2 cm.

The amorphous state of the glasses was checked by X-ray diffraction using Xpert PRO'panalytical X-ray diffractometer with CuK_α radiation. Scanning electron microscopy studies were also carried out on these samples to observe the crystallinity if any using HITACHI S-3400N Scanning Electron Microscope. The energy dispersive spectroscopy measurements were conducted on a Thermoinstruments Model Noran system 6 attached to scanning electron microscope. Thermal analysis of these samples was carried out (by TA instruments Model Q20 V24.2 Build 107) with the heating rate of 10 °C/min in the temperature range 30–800 °C. The density of the glasses was determined to an accuracy of (±0.0001) by the standard principle of Archimedes' using o-xylene (4N pure) as the buoyant liquid. The mass of the samples was measured to an accuracy of 0.1 mg using Ohaus digital balance Model AR2140 for evaluating the density. The refractive index n_d of the glasses was measured (at λ = 589.3 nm) using Abbe refractometer with monobromo naphthalene as the contact layer between the glass and the refractometer prism. Infrared transmission spectra were recorded on a JASCO-FT/IR-5300 spectrophotometer to a resolution of 0.1 cm^{-1} in the spectral range 400–2000 cm^{-1} using potassium bromide pellets (300 mg) containing pulverized sample (1.5 mg). These pellets were pressed in a vacuum die at ~680 MPa. The Raman spectra were recorded on an NIR excitation line (1064 nm) using a Bio-Rad spectrometer FTS 175C equipped with an FT Raman supplementary accessory working in a back-scattering geometry system.

The optical absorption spectra of the glasses were recorded at room temperature in the spectral wavelength range covering 400–2300 nm to a spectral resolution of 0.1 nm using JASCO Model V-670 UV–vis–NIR spectrophotometer. The luminescent spectra of the samples were recorded at room temperature on a Photon Technology International (PTI) Spectrofluorometer. This instrument contains autocalibrated quadrascopic monochrometer for wavelength selection and quadracentric sample compartment. The light source is high intensity continuous xenon lamp with high sensitivity TE-cooled InGaAs detector with lock-in amplifier and chopper for noise suppression and an additional emission mono with a 600 groove grating blazed at 1.2 μm. The system provides unmatched NIR luminescence recording capability from 500 to 2.2 μm. The other details of luminescence recording were reported in our earlier papers [39,40]. The fluorescence decay curves were recorded using Jobinyvon spectrofluorolog-3 with pulsed xenon lamp of 450 W. The electron spin resonance (ESR) spectra of the coarsely powdered samples were recorded at room temperature on JEOL JES-TES100 X-band EPR spectrometer; the magnetic field was kept at 5 mT/min and modulated at 100 kHz.

3. Results

From the measured values of density d and calculated average molecular weight $\overline{M}$, various physical parameters such as rare earth ion concentration N_i and mean Ln ion separation r_i of these glasses

Table 1
Physical parameters of ZnF_2–WO_3–TeO_2:Ln_2O_3 glasses.

Physical Parameter	Nd^{3+} doped glasses				Sm^{3+} doped glasses				Eu^{3+} doped glasses			
	NdW_5	NdW_{10}	NdW_{15}	NdW_{20}	SmW_5	SmW_{10}	SmW_{15}	SmW_{20}	EuW_5	EuW_{10}	EuW_{15}	EuW_{20}
Density d (g/cm^3)	5.505	5.616	5.726	5.837	5.525	5.636	5.746	5.857	5.618	5.729	5.839	5.950
Molar volume V_m (cm^3/mol)	25.37	26.02	26.63	27.23	25.30	25.95	26.57	27.16	24.89	25.53	26.14	26.74
Refractive index (n_d)	1.501	1.502	1.502	1.503	1.504	1.505	1.506	1.507	1.512	1.514	1.515	1.515
Ln^{3+} ion conc. N_i (10^{19} ions/cm^3)	1.19	2.31	3.39	4.42	1.19	2.32	3.40	4.43	1.21	2.36	3.46	4.50
Inter-ionic distance r_i (nm)	9.44	7.56	6.66	6.09	9.44	7.55	6.65	6.09	9.38	7.51	6.61	6.06
Polaron radius r_p (nm)	3.81	3.05	2.68	2.45	3.78	3.03	2.67	2.44	3.80	3.04	2.68	2.45

are evaluated using the conventional formulae and are presented in Table 1.

SEM pictures and X-ray diffraction pattern of the ZnF_2–WO_3–TeO_2:Ln_2O_3 glass samples showed no signs of crystallinity, indicating the prepared samples were of amorphous in nature. The chemical makeup of the glasses is evaluated using EDS. In Fig. 2, EDS of one of the glass samples in each series viz., LnW_{10}:$40ZnF_2$–$10WO_3$–$49TeO_2$:$1Ln_2O_3$ are presented; the analysis indicates the presence of Te, Zn, O, F, W, Nd, Sm and Eu elements in the glass samples.

In Fig. 3, differential scanning calorimetric (DSC) scans of ZnF_2–WO_3–TeO_2 glass doped with Nd_2O_3 are presented. The trace of the glass NdW_5 exhibited an endothermic effect due to glass transition at about 300 °C followed by a well-defined exothermic effect due to crystallization temperature (T_C). The trace also exhibited another endothermic effect due to melting at 620 °C. The variation of glass transition temperature (T_g), and glass forming ability parameter $K_{gl} = (T_C - T_g)/(T_m - T_C)$ with the concentration of WO_3 for the three rare earth doped glasses are shown as inset of Fig. 3. The variation shows a downward kink at 15 mol% of WO_3.

Fig. 4 shows infrared transmission spectra of ZnF_2–WO_3–TeO_2:Sm_2O_3 glasses. The spectra exhibited different absorption bands due to various structural units of TeO_2 and WO_3. IR spectrum of crystalline TeO_2 (inset of Fig. 4) exhibited two absorption bands at 772 cm^{-1} [$\nu_1(A_1)$] and at 650 cm^{-1} [$\nu_2(A_2)$] due to ν_s-TeO_{2eq} and ν_s-TeO_{2ax} vibrations with C_{2v} symmetry, respectively [41]. In the spectrum of glass SmW_5 (Fig. 4), the vibrational frequency of ν_s-TeO_{2ax} (axial band) is located at 645 cm^{-1} whereas the ν_s-TeO_{2eq} is observed to be missing. Additionally, the spectrum of this glass exhibited the bands due to ν_1 and ν_4 vibrations of WO_4 groups

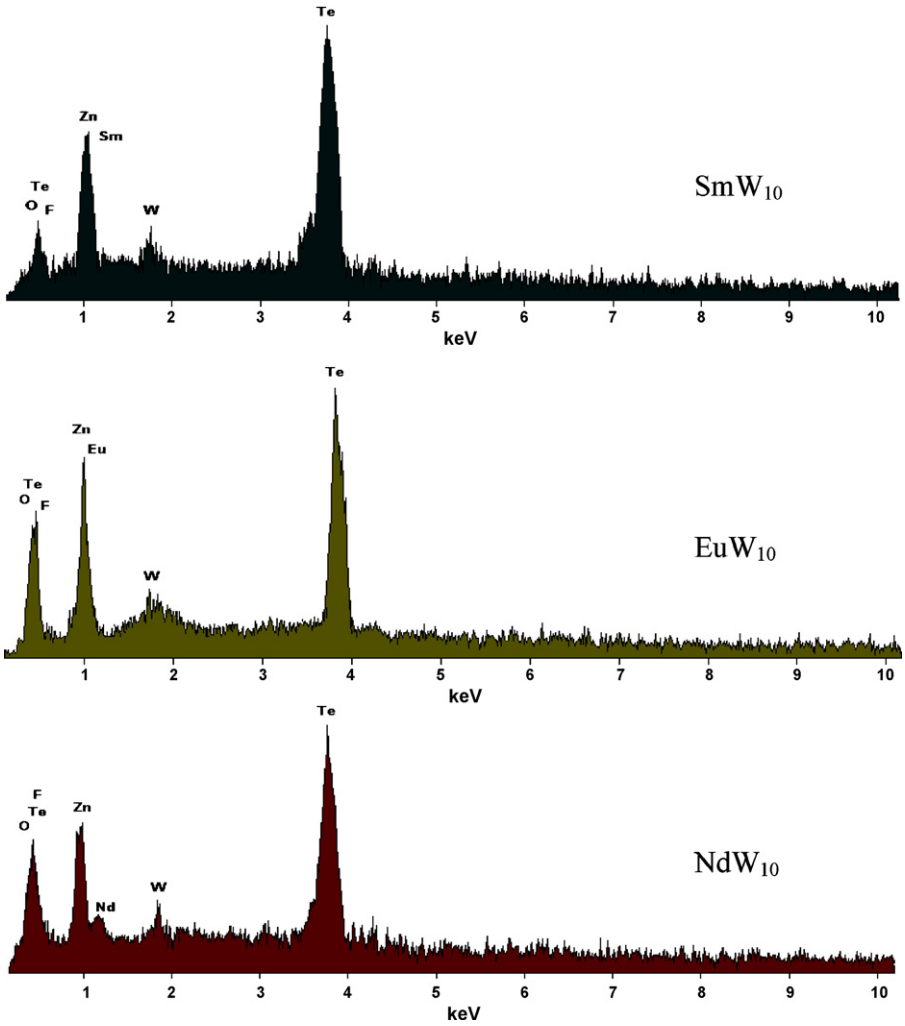

Fig. 2. Energy dispersive spectra of ZnF_2–WO_3–TeO_2:Ln_2O_3 glasses mixed with 10 mol% of WO_3.

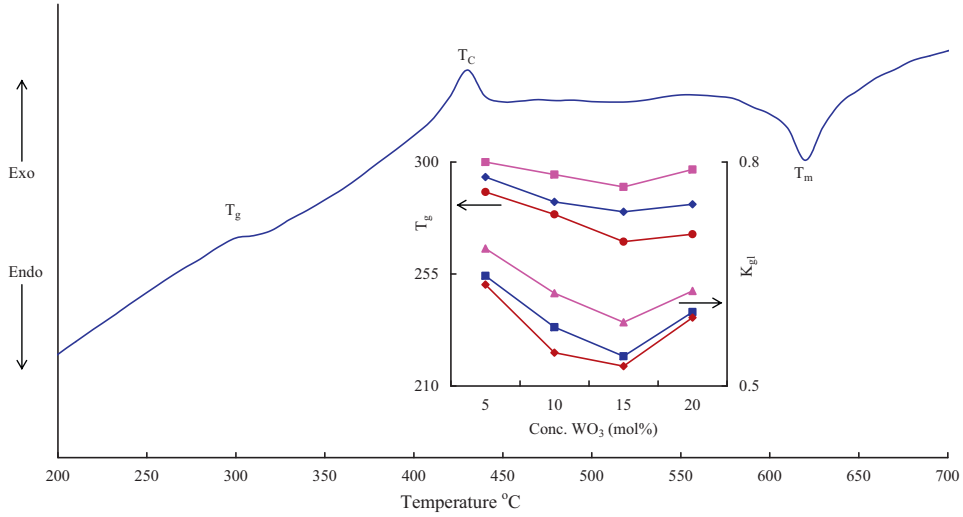

Fig. 3. Differential scanning calorimetric (DSC) scans of ZnF_2–TeO_2:Nd_2O_3 glass mixed with 10 mol% of WO_3. Inset represents variation of glass forming ability parameter with the concentration of WO_3 for the three rare earth doped glasses.

at 936 and 421 cm^{-1} respectively and also a feeble band at about 966 cm^{-1} due to ν_1 vibrations of WO_6 groups [42]. As the concentration of WO_3 is increased, the band due to WO_6 group is observed to grow at the expense of band due to WO_4 groups. The symmetrical equatorial band of TeO_2 is also observed to decay gradually with the increase in the concentration of the WO_3 at least up to 15 mol%. A similar behaviour is exhibited by the spectra of other two series of glasses.

In Fig. 5, the Raman spectra of ZnF_2–WO_3–TeO_2 glasses doped with Eu^{3+} ions are presented. The spectrum of glass EuW_5 exhibited a band at about 480 cm^{-1} assigned to the stretching vibrations of Te–O–Te linkages between TeO_4 trigonal bipyramids (tbp) and another intense band at 685 cm^{-1} assigned to Te–O stretching vibration of TeO_4 tbp units. Yet, another significant band at about 750 cm^{-1} due to $[TeO_{3+1}]^{4-}$, $[TeO_3]^{2-}$ units [43–46] is also located in the spectra. The spectrum also exhibited bands at 376 cm^{-1} due to the bending vibrations of W–O–W linkages of WO_6 units [47]. The band due to $W–O^-$ stretchings in the WO_4 units is also observed at about 950 cm^{-1}. As the content of WO_3 is increased up to 15 mol%, the intensity of the bands due to WO_6, $[TeO_{3+1}]^{4-}$, $[TeO_3]^{2-}$ units is observed to increase gradually where as that of bands due to TeO_4 and WO_4 structural units is observed to decrease. The spectra of the other two series of the glasses exhibited similar behaviour.

Fig. 6 shows typical ESR spectra (recorded at room temperature) of ZnF_2–TeO_2:Nd_2O_3 glasses mixed with different concentrations of WO_3; the spectra exhibited an asymmetric signal (signal 1) identified due to W^{5+} ions [48] at $g_\perp \sim 1.71$ and $g_{||} \sim 1.62$ and another signal (signal 2) at higher magnetic fields which is typical for oxygen (paramagnetic O^- ions) defects [49]. The intensity and half-width of these signals are observed to be maximal in the spectrum of the glass NdW_{15}. The ESR spectra were observed to be similar for other two series of glasses.

Optical absorption spectra of the three rare earth ion doped glass samples have exhibited the bands due to the following transitions (Fig. 7(a)–(c)).

$$Nd^{3+}: {}^4I_{9/2} \rightarrow {}^2P_{1/2}, {}^2K_{15/2} + {}^2G_{9/2} + {}^2D_{3/2} + {}^4G_{11/2}, {}^4G_{9/2}, {}^2K_{13/2} + {}^4G_{7/2}, {}^4G_{5/2} + {}^2G_{7/2}, {}^2H_{11/2}, {}^4F_{9/2}, {}^4F_{7/2} + {}^4S_{3/2}, {}^4F_{5/2} \text{ and } {}^4F_{3/2}$$

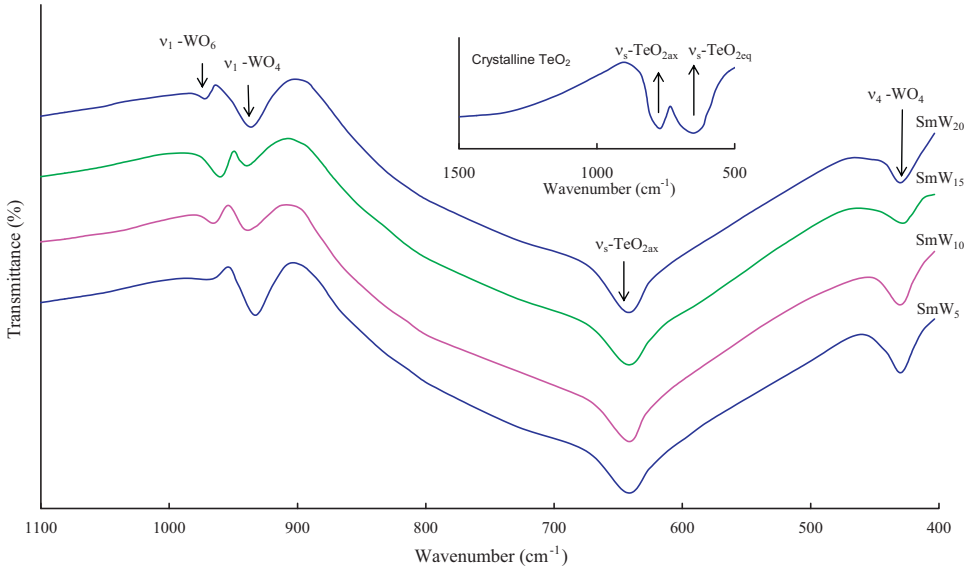

Fig. 4. IR spectra of ZnF_2–WO_3–TeO_2:Sm_2O_3 glasses mixed with different concentrations of WO_3.

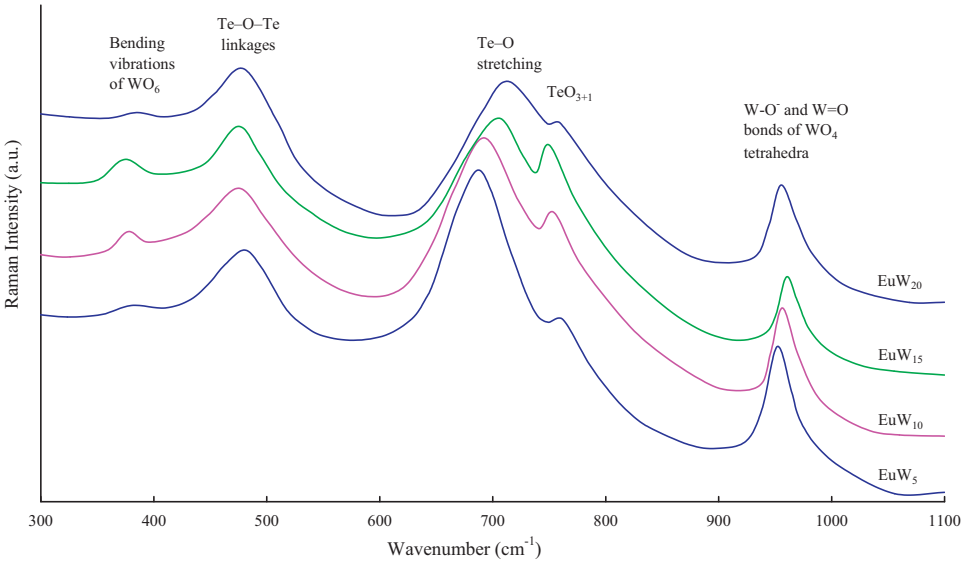

Fig. 5. Raman spectra of ZnF_2–WO_3–TeO_2:Eu_2O_3 glasses mixed with different concentrations of WO_3.

Sm^{3+}: $^6H_{5/2} \rightarrow {}^4I_{13/2}, {}^4I_{11/2}, {}^6F_{11/2}, {}^6F_{9/2}, {}^6F_{7/2}, {}^6F_{5/2}, \times {}^6F_{3/2}, {}^6H_{15/2}$ and $^6F_{1/2}$,

Eu^{3+}: $^7F_0 \rightarrow {}^5D_2, {}^7F_6, {}^7F_5$ and $^7F_1 \rightarrow {}^5D_1$

With the increase in the concentration of WO_3, considerable variations in the spectral peak positions and the intensity of the bands have been observed. Additionally, a weak broad band at about 1030 nm presumably due to the transitions of W^{5+} ions is also observed in the spectra of these glasses with maximum intensity for LnW_{15} glasses (Fig. 7(b)).

The experimental oscillator strengths (OS) of the absorption transitions were estimated from the spectra for all the three rare earth ion doped glasses in terms of the area under absorption peaks. The OS of the electric dipole transition between two states have been calculated using the J–O theory, with the conventional equation [50,51]:

$$f_{\text{cal}} = \frac{8\pi mc\nu\chi}{3h(2J+1)} \sum_{\lambda=2,4,6} \Omega_\lambda \langle f^N[\gamma, S, L]J||U^\lambda||f^N[\gamma', S', L']J'\rangle \quad (1)$$

with the symbols have their usual meaning.

The procedure of fitting of the calculated OS from Eq. (1) to those evaluated from the experimental spectra is described in Ref. [52]. A set of matrix equations (which includes the U^2, U^4, and U^6 matrices, the matrices of the experimental OS and the energies of the corresponding transitions) have been solved to minimize the difference between the calculated f_{calc} and observed f_{exp} OS. The quality of fitting is determined by the root mean squared deviation and presented in Table 2a and b for Nd^{3+} and Sm^{3+} doped glasses. The deviation indicates reasonably good fitting between theory and experiment demonstrating the applicability of J–O theory.

The summary of the J–O parameters Ω_λ for the rare earth ion (Nd^{3+} and Sm^{3+}) doped ZnF_2–WO_3–TeO_2 glasses is presented in Table 3a and b.

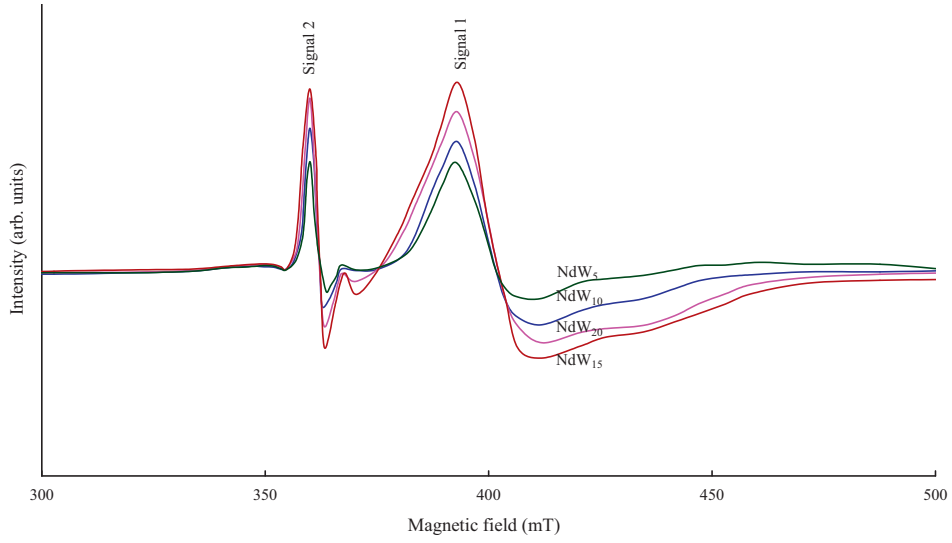

Fig. 6. ESR spectra of ZnF_2–WO_3–TeO_2:Eu_2O_3 glasses mixed with different concentrations of WO_3.

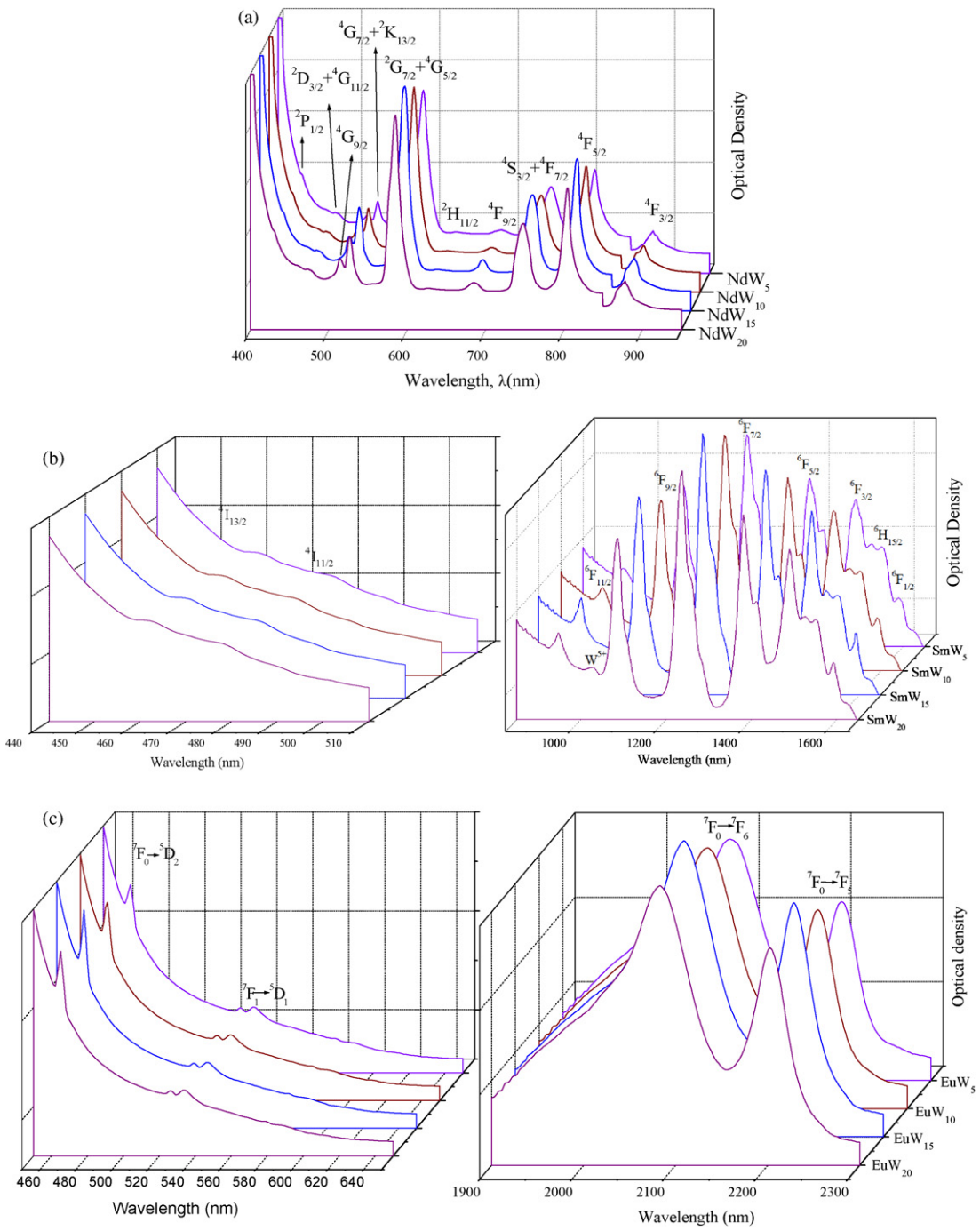

Fig. 7. (a) Optical absorption spectra of ZnF_2–WO_3–TeO_2:Nd_2O_3 glasses. (b) Optical absorption spectra of ZnF_2–WO_3–TeO_2:Sm_2O_3 glasses. (c) Optical absorption spectra of ZnF_2–WO_3–TeO_2:Eu_2O_3 glasses.

However, for Eu^{3+} doped glasses, Judd–Ofelt intensity parameters have been calculated directly from the emission spectra since the well resolved absorption bands could not be observed in the visible region.

The bonding parameter (δ), defined as [53,54]

$$\delta = \frac{1-\bar{\beta}}{\bar{\beta}} \times 100, \tag{2}$$

is computed for all the three series of glasses. In Eq. (2), $\bar{\beta} = \sum_{1N}\beta/N$ and β (the nephelauxetic ratio) = ν_c/ν_a. ν_c and ν_a are the energies in cm^{-1} of the corresponding transitions in the complex and aquo-ion respectively and N refers to the number of levels used to compute $\bar{\beta}$ values. The computation shows a slight decrease of δ value with the increase of WO_3 up to 15 mol% (Table 3).The luminescence spectra of all the three series of glasses recorded at room temperature in the visible and NIR regions are shown in Fig. 8(a)–(c). The spectra exhibited the following prominent emission bands:

Nd^{3+} (λ_{exc} = 878 nm) : $^4F_{3/2} \rightarrow {}^4I_{9/2}, {}^4I_{11/2}, \mathbf{{}^4I_{13/2}}$

Sm^{3+} (λ_{exc} = 462 nm) : $^4G_{5/2} \rightarrow {}^6H_{5/2}, \mathbf{{}^6H_{7/2}}, {}^6H_{9/2}$

Eu^{3+} (λ_{exc} = 465 nm) : $^5D_0 \rightarrow {}^7F_0, {}^7F_1, \mathbf{{}^7F_2}, {}^7F_3, {}^7F_4$

Table 2
The absorption band energies and the values of the experimental ($f_{exp} \times 10^6$), and calculated ($f_{calc} \times 10^6$) oscillator strengths and root mean square deviation (r.m.s.) of Ln^{3+} ion in ZnF_2–TeO_2 glasses mixed with different concentrations of WO_3.

Band	NdW_5			NdW_{10}			NdW_{15}			NdW_{20}		
	ν (cm^{-1})	f_{exp}	f_{calc}	ν (cm^{-1})	f_{exp}	f_{calc}	ν (cm^{-1})	f_{exp}	f_{calc}	ν (cm^{-1})	f_{exp}	f_{calc}
(a) Nd^{3+} ion												
$^2K_{15/2} + {}^2G_{9/2} + {}^2D_{3/2} + {}^4G_{11/2}$	21,148.8	4.135	4.265	21,079.1	4.203	4.546	21,034.5	4.789	4.842	21,057.1	4.468	4.751
$^4G_{9/2}$	19,652.5	4.336	4.591	19,558.2	4.035	4.947	19,529.3	5.024	4.984	19,533.2	4.598	4.487
$^2K_{13/2} + {}^4G_{7/2}$	18,958.1	11.157	14.568	18,918.9	10.362	16.187	18,885.7	16.425	16.985	18,905.7	14.856	17.054
$^4G_{5/2} + {}^2G_{7/2}$	17,128	82.045	82.926	17,101.5	84.554	84.110	17,094.6	86.754	86.592	17,099.9	85.492	85.843
$^2H_{11/2}$	15,860.4	0.103	0.210	15,836.6	0.114	0.538	15,796.5	0.213	0.305	15,820.3	0.208	0.254
$^4F_{9/2}$	14,661.6	3.059	2.843	14,607.8	3.438	2.341	14,537.0	3.925	2.982	14,577.3	3.834	3.715
$^4F_{7/2} + {}^4S_{3/2}$	13,426.4	22.583	22.847	13,385.9	23.996	26.025	13,355.1	25.648	26.285	13,372.6	25.317	25.745
$^4F_{5/2}$	12,478.2	24.678	23.148	12,423.6	25.776	20.243	12,367.1	26.084	25.892	12,400.8	26.824	26.158
$^4F_{3/2}$	11,415.5	7.308	7.273	11,369.3	7.739	7.544	11,350.2	8.124	8.087	11,361.1	8.182	7.806
	r.m.s.	1.289				0.763			0.433		0.805	

Band	SmW_5			SmW_{10}			SmW_{15}			SmW_{20}		
	ν (cm^{-1})	f_{exp}	f_{calc}	ν (cm^{-1})	f_{exp}	f_{calc}	ν (cm^{-1})	f_{exp}	f_{calc}	ν (cm^{-1})	f_{exp}	f_{calc}
(b) Sm^{3+} ion												
$^6F_{11/2}$	10,565	0.785	0.915	10,541	0.801	1.031	10,523	1.145	1.031	10,530	0.953	1.053
$^6F_{9/2}$	9220	6.026	6.157	9195	5.946	6.327	9181.1	6.283	6.327	9185	6.276	6.624
$^6F_{7/2}$	8056	8.246	8.734	8043	9.658	9.281	8030.8	10.295	9.281	8035	10.163	10.053
$^6F_{5/2}$	7213	4.907	5.017	7209	5.360	5.113	7197.9	5.452	5.692	7202	5.386	5.475
$^6F_{3/2}$	6744	1.248	1.833	6732	1.548	2.488	6721.3	2.205	2.819	6726	1.982	2.108
$^6F_{1/2} + {}^6H_{15/2}$	6445	1.148	0.751	6431	1.008	0.328	6419.3	1.352	1.407	6425	1.342	1.291
	r.m.s.	0.361			3.446			0.497			0.168	

It is noticed that with increase in the content of WO_3 up to 15 mol%, the intensity of the three principal bands viz., $^4F_{3/2} \rightarrow {}^4I_{13/2}$ (Nd^{3+}), $^4G_{5/2} \rightarrow {}^6H_{7/2}$ (Sm^{3+}), $^5D_0 \rightarrow {}^7F_2$ (Eu^{3+}) is observed to increase.

The energy level diagrams containing observed absorption and emission transitions of Nd^{3+}, Sm^{3+} and Eu^{3+} ions for one of the glasses (glass containing 10 mol% WO_3) in each series are shown in Fig. 9.

Using J–O intensity parameters, the radiative transition probability from the excited state $\langle f^N[\gamma, S, L]J|$ to the lower state $|f^N[\gamma', S', L']J'\rangle$ is evaluated by the standard equation:

$$A_{JJ'} = \frac{64\pi^4 e^2 \nu^3}{3h(2J'+1)} \left[\frac{n(n^2+2)^2}{9} S_{ed}\right] \quad (3)$$

where

$$S_{ed} = \sum_{\lambda=2,4,6} \Omega_\lambda \langle f^N[\gamma, S, L]J||U^\lambda||f^N[\gamma', S', L']J\rangle^2,$$

and e is the charge of electron, and all other quantities are the same as in Eq. (2). Summing up the $A_{JJ'}$ quantities over all possible final states, one can get the radiative life time τ of an excited energy level and the branching ratio $\beta_{JJ'}$ are evaluated using as,

$$\tau = \frac{1}{\sum_{J'} A_{JJ'}} \quad (4)$$

$$\beta_{JJ'} = \frac{A_{JJ'}}{\sum_{J'} A_{JJ'}} \quad (5)$$

The details of emission parameters for the glasses mixed with 10 mol% of WO_3 for all the three rare earth doped glasses are presented in Tables 4a–4c and the summary of these data for the three principal levels in Table 5.

Since the matrix elements of the unit tensor operators for the $^5D_0$–$^7F_3$ transition for this ion are zero, estimation of the radiative transition probability could not be possible.

4. Discussion

It is well known that the basic building block of TeO_2 glass structure is a trigonal bipyramid commonly called TeO_4 *E*, where one of the three equatorial directions is occupied by the $5s^2$ electronic pair (*E*) of the tellurium atom with two equatorial bonds. The environment of these Te atoms is completed by two other longer interactions of lengths 2.9 Å and the three dimensional close packing is constituted from vertices sharing TeO_4 groups (Te_{eq}–O_{ax}–Te) reinforced by weaker Te–O interactions of lengths 2.9 Å [41,55]. In general ZnF_2 acts as modifier, fluorine ions break the Te–O bonds while Zn^{2+} ions may occupy interstitial positions or may form Zn–O–Te linkages because of the close ionic radii of Te^{4+} (0.7 Å) and Zn^{2+} (0.74 Å) ions.

Table 3
Summary of the J–O parameters Ω_λ for the rare earth ion doped ZnF_2–WO_3–TeO_2 glasses.

Glass	Ω_2	Ω_4	Ω_6	Ω_4/Ω_6	δ
(a) Nd^{3+} doped glasses					
NdW_5	26.85	17.69	21.67	0.82	0.876
NdW_{10}	24.55	15.07	19.23	0.78	0.824
NdW_{15}	20.63	13.56	18.83	0.72	0.792
NdW_{20}	22.45	14.10	17.72	0.80	0.807
(b)Sm^{3+} doped glasses					
SmW_5	0.96	15.47	9.62	1.61	−0.0916
SmW_{10}	0.91	10.17	7.66	1.33	−0.0959
SmW_{15}	0.82	9.15	7.15	1.28	−0.1060
SmW_{20}	0.90	9.65	7.28	1.32	−0.0972

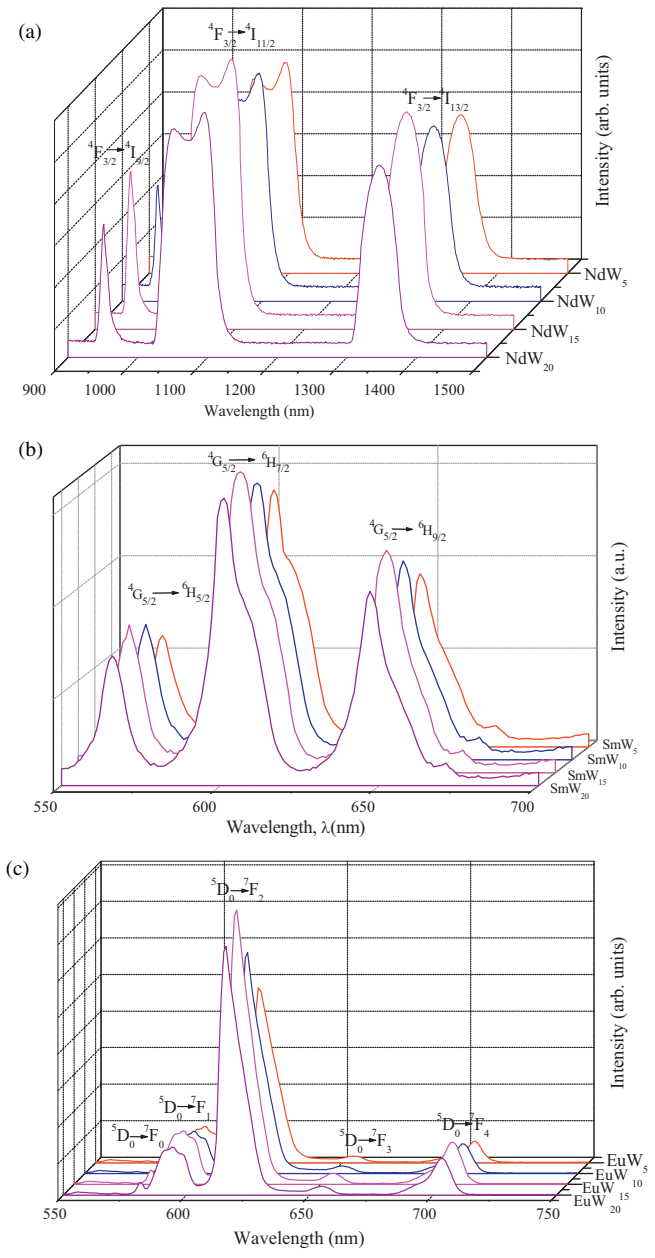

Fig. 8. (a) Photoluminescence spectra of ZnF_2–WO_3–TeO_2:Nd_2O_3 glasses recorded at room temperature (λ_{exc} = 878 nm). (b) Photoluminescence spectra of ZnF_2–WO_3–TeO_2:Sm_2O_3 glasses recorded at room temperature (λ_{exc} = 462 nm). (c) Photoluminescence spectra of ZnF_2–WO_3–TeO_2:Eu_2O_3 glasses recorded at room temperature (λ_{exc} = 465 nm).

WO_3 belongs to the intermediate class of glass forming oxides. It is an incipient glass network former, normally tungsten ion exists in W^{6+} state and participates in glass network with WO_4 and WO_6 structural units and may alternate with tellurite structural units and form the linkages of the type Te–O–W as mentioned earlier [56,57]. Tungsten ions also exist in stable W^{5+} state, form $W^{5+}O_3$ complexes and occupy octahedral positions with distortions due to the Jahn–Teller effect [58] and decrease the long-range ordering in the glass network. Brenier and Kityk have demonstrated that such a decease in the long-range orders leads to a substantial widening of the emission peaks of rare earth ions present in the glass matrix [59]. A weak kink (at 1030 nm Fig. 7) observed in the optical absorption spectra of with the highest intensity in the glasses LnW_{15} is identified due to $d_{xy} \rightarrow d_{x^2-y^2}$ transition of W^{5+} ions indicating conversion of a part of tungsten ions into W^{5+} state.

The observed increase in the half width and the intensity of the ESR signal with the concentration of WO_3 up to 15 mol% obviously suggests the gradual hike in the concentration of W^{5+} ions in the glass matrix. The value of g factor observed in the range $1.65 < g_{\perp} < 1.75$ and $1.55 < g_{||} < 1.65$ indicate that W^{5+} ions present in axially distorted octahedral positions with a short W–O bond and an opposite long W–O bond along the symmetry axis of oxygen ions [57]. Additionally the difference between $g_{||}$ and $g_{\perp}$ (anisotropy factor) changes is different for different for rare earth ion doped glasses in the glass network; this observation indicates that W^{5+} octahedron experiences different structural changes for different rare earth ion doped glasses.

Overall, there is a gradual increase in structural depolymerization in the glasses with increase in the content of WO_3 up to 15 mol%. This result is also consistent with the variations in T_g and $T_c - T_g$ values observed in the DSC studies. With increase in the concentration of WO_3 up to 15 mol%, the glass transition temperature T_g and the glass forming ability parameter have exhibited a decreasing trend. Such trend indicates the lessening of augmented cross-link density of various structural groups and closeness of packing.

Yet, another support for this argument can also be obtained from IR and Raman spectra. In these spectra it is observed that the symmetrical vibrational frequencies of $\nu_{ax}{}^s$-TeO_2 bonds of TeO_4 groups in the IR spectra are spectrally shifted towards higher frequencies with decreasing intensity as the concentration of WO_3 is increased up to 15 mol%. The intensity of the bands due to WO_6 structural units is observed to increase at the expense of the band due to WO_4 structural units. As per the earlier reports the octahedrally positioned tungsten ions induce non-bridging oxygens where as tetrahedral tungsten ions participate in the glass network [57]. Thus the results of IR and Raman spectra suggest that there is an increasing degree of disorder owing due to increasing content of modifying W^{5+} ions.

The W^{5+} ions are expected to occupy only interstitial positions and act as modifiers since the ratio of cation–oxygen radii is 0.45 for W^{5+} ion, which is far from the value of 0.19 possessed by an ion to occupy tetrahedral or substitutional sites [60]. These ions enter the glass network by breaking up W–O–Te and Te–O–Te bonds and introduce: (i) the stable $Te–O^-$ and (ii) unstable $Te–O^-$ bonds which will later be modified to $Te–O^-$ (or simply TeO_{3+1}) owing to the contraction of one $Te–O^-$ and the elongation of another $Te–O^-$ bond as illustrated in Fig. 10. With increasing WO_3 content (up to 15 mol%), cleavage of continuous network leads to an increase in the fraction of TeO_{3+1} polyhedra. Further, the elongation of Te–O bond of TeO_{3+1} and its cleavage finally lead to the formation of trigonal prismatic TeO_3 units. Thus in addition to Te–O–Te, W–O–Te linkages, WO_4 and WO_6 units, the structure of the studied glass network consists of TeO_{3+1} and TeO_3, free Zn^{2+} ions, free F^- ions and non-bridging oxygens. The concentration of such bonding defects as mentioned above depends upon the concentration of WO_3.

Thus, the variation in the concentration of WO_3 causes substantial structural modifications at the lasing ion site in ZnF_2–WO_3–TeO_2 glass network. If we consider the varying concentrations of tungsten ions of different valence states to be incorporated between the long-chain molecules in the vicinity of rare earth ion in the Te–O–Te network, then the symmetry and/or covalency of the glass at the rare earth ions should be different for the glasses containing different concentrations of WO_3 in the glass network. Additionally, the variations in the concentration of different structural units of tellurite, tungstenate and linkages between them are also expected to modify the crystal field around lasing ions in the glass network.

The rare earth ions that occupy different coordination sites with non-centro symmetric potential contribute significantly to Ω_2. Even with similar coordination, the differences in the distor-

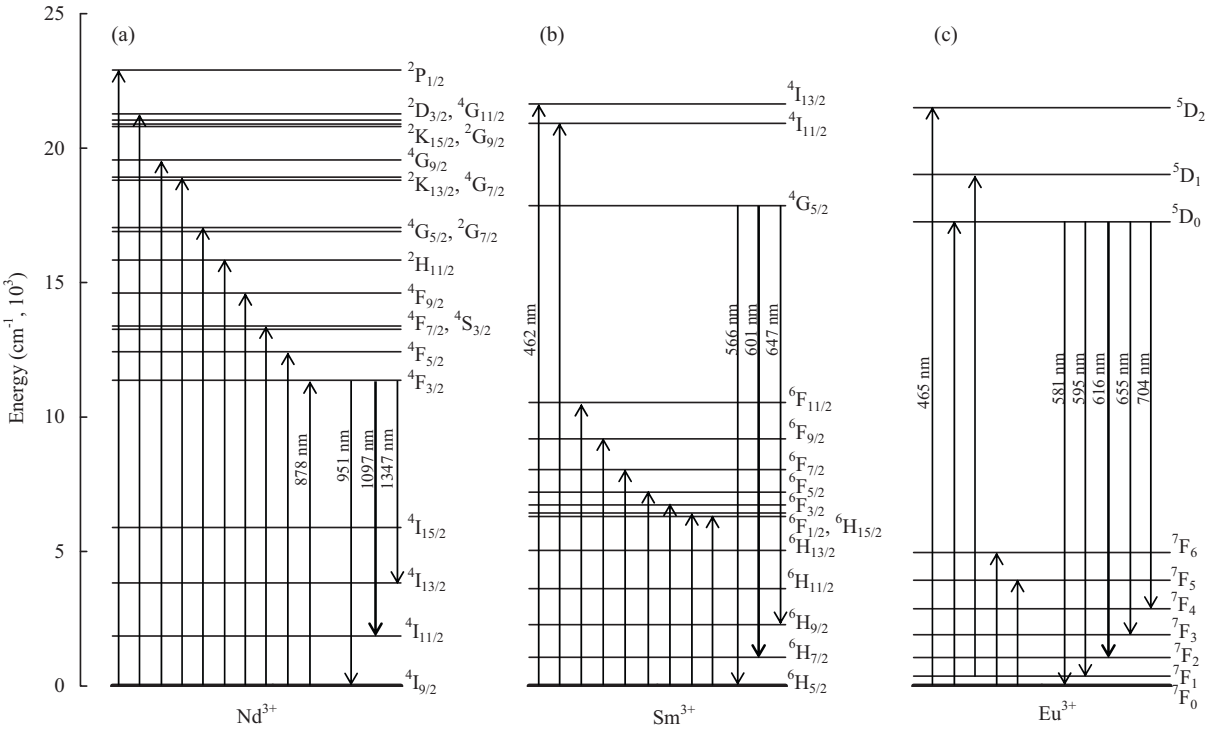

Fig. 9. The energy level diagrams containing observed absorption and emission transitions of Nd^{3+}, Sm^{3+} and Eu^{3+} ions in ZnF_2–TeO_2 glasses mixed with 10 mol% of WO_3.

tion at these ion sites may lead to a distribution in the local crystal field. The variations in the sites with non-centro symmetric potential (that may arise due to the influences of the dielectric of media, the environment of the rare earth ion and nephelauxetic effect) lead to changes in Ω_2 value. In fact, among the three J–O parameters, the parameter Ω_2 is related to the covalency and structural changes in the vicinity of the rare earth ion (short-range effect) and Ω_4 and Ω_6 are related the long-range effects and are strongly influenced by the vibrational levels associated with the central rare earth ions bound to the ligand atoms. The comparison of Ω_2 parameter for the three rare earth doped glasses shows the lowest values for glasses mixed with 15 mol% of WO_3.

According to the Judd–Ofelt theory, the intensity parameters contain two terms: (i) crystal field parameter that determines the symmetry and distortion related to the structural change in the vicinity of Ln^{3+} ions. In the present context, this may be understood as follows: the higher the concentration of the modifier ions (W^{5+} ions), the larger is the average distance between Te–O–W, Te–O–Te chains causing the average Ln–O distance to increase. Such increase in the bond lengths produces weaker field around Ln^{3+} ions leading to a decrease in the value of Ω_2 with increase in the concentration of WO_3. (ii) The covalency between the Ln^{3+} ion and the ligand oxygen ion also contribute to Ω_2. For oxide glasses this is related to the radial overlapping integral of the wavefunctions between 4f and admixing levels, e.g. 5d, 5g and the energy denominator between these two energy terms. Thus decreasing value of Ω_2 with increase in the concentration of WO_3 up to 15 mol% points out, that there is a gradual increase in the concentration of W^{5+} ions that act as modifiers in all the three series of the glasses. The values of Ω_4 and Ω_6 are strongly influenced by the vibrational levels associated with the central rare earth ions bound to the ligand atoms. The bonding parameter δ evaluated from the absorption data showed a decreasing trend with increase in the concentration of WO_3 up to 15 mol%. This observation indicates a decreasing covalent environment for Ln^{3+} ions from glass LnW_5 to LnW_{15} and slightly higher covalent environment in glass LnW_{20} with respect to that in LnW_{15}.

In the absorption spectra of Nd^{3+} doped samples, the transition $^4I_{9/2} \rightarrow {}^4G_{5/2}$ is found to be more intense than any other state. This is evidently because of better validity of the selection rules, $\Delta J < 2$, $\Delta L < 2$ and $\Delta S = 0$, for this transition. In addition, the higher values of $||U^{\lambda}||^2$ are also considered as an important factor for the hyper sensitive nature of this level [61]. The positions of $^4I_{9/2} \rightarrow {}^4G_{5/2}$, $^4G_{7/2}$ transition of Nd^{3+} are spectrally shifted towards slightly longer wavelength with the increase of WO_3 content. This observation indicates the dwindling of covalency of the chemical bond between the Nd^{3+} and the ligand atoms [61]. This is also in accordance with the trend in Ω_2. We have also observed the effective bandwidth of these transitions to be the highest for the glasses mixed with 15 mol% of WO_3. This observation points out that the distribution in the crystal fields due to differences in the site symmetries of Nd^{3+} is narrower for the NdW_{15} glass compared to the other three glasses in this series [19]. From the energy range of the transition $^4I_{9/2} \rightarrow {}^2P_{1/2}$ (23,200–23,400 cm^{-1}) observed, the effective coordination of this ion may be assumed between 8 and 9 in the studied glass network [20]. The eight coordination with C_2 symmetry may visualized by four pairs of oxide ions coming from four tetrahedral constituted by TeO_4 and WO_4 units as illustrated in Fig. 10.

The optical transitions $^6H_{5/2} \rightarrow {}^6F_{9/2}$, $^6F_{7/2}$ of Sm^{3+} occurring in the absorption spectra in the near infrared region are hypersensitive. In the emission spectra of Sm^{3+} ion, the transition $^4G_{5/2} \rightarrow {}^6H_{9/2}$ is also identified as hypersensitive. The closer observation of these spectra further indicates that $^6H_{5/2} \rightarrow {}^6F_{7/2}$ transition is a threefold triplet. Due to certain self adjustment of Sm^{3+} environment in the glass network, there may be a degeneracy of $^6H_{5/2}$ ground state in the crystal field [62]; such degeneracy leads to the observed splitting of this transition. The luminescence spectra of Sm^{3+} are similar to those reported for a number of other glass systems [62–64]. The high intensity of the luminescence bands of Sm^{3+} ion in SmW_{15} glass indicates the quenching of luminescence in this glass is low. The high luminescence output obtained for this glass also indicates that there is a less cross relax-

Table 4a
Radiative parameters of Nd^{3+} doped ZnF_2–TeO_2 glasses mixed with 10 mol% of WO_3.

Initial state and calculated radiative lifetime	Final state	ν (cm^{-1})	Radiative probability A (s^{-1})	Branching ratio β%
$^2K_{15/2} + {}^2G_{9/2} + {}^2D_{3/2} + {}^4G_{11/2}$ $\tau = 12$ μs	$^4I_{9/2}$	21,079	3635.0	44.0
	$^4I_{11/2}$	19,222	9268.6	11.22
	$^4I_{13/2}$	17,243	22,030	26.67
	$^4I_{15/2}$	15,183	37,195	45.03
	$^4F_{3/2}$	9710.1	591.73	0.72
	$^2H_{9/2}$	9028.1	3400.5	4.12
	$^4F_{5/2}$	8655.5	874.32	1.06
	$^4F_{7/2} + {}^4S_{3/2}$	7693.2	1865	2.25
	$^4F_{9/2}$	6472.1	2033.7	2.46
	$^2H_{11/2}$	5242.5	1492.8	1.81
	$^4G_{5/2} + {}^2G_{7/2}$	3977.6	150.2	0.18
	$^2K_{13/2} + {}^4G_{7/2}$	2160.2	25.664	0.03
			24.804	0.03
	$^4G_{9/2}$	1520.9	13.041	0.02
			$\sum_{J'} A_{JJ'} = 82601$	
$^4G_{9/2}$ $\tau = 22$ μs	$^4I_{9/2}$	19,558	2847.4	6.16
	$^4I_{11/2}$	17,701	11,748	25.41
	$^4I_{13/2}$	15,722	25,402	54.94
	$^4I_{15/2}$	13,662	3809.6	8.24
	$^4F_{3/2}$	8189.2	444.13	0.96
	$^2H_{9/2}$	7507.2	291.85	0.63
	$^4F_{5/2}$	7134.6	499.24	1.08
	$^4F_{7/2} + {}^4S_{3/2}$	6172.3	938.99	2.0
	$^4F_{9/2}$	4951.2	163.04	0.35
	$^2H_{11/2}$	3721.6	55.32	0.12
	$^4G_{5/2} + {}^2G_{7/2}$	2456.7	33.9	0.08
	$^2K_{13/2} + {}^4G_{7/2}$	639.30	0.51	0.0
			$\sum_{J'} A_{JJ'} = 46234$	
$^2K_{13/2} + {}^4G_{7/2}$ $\tau = 23$ μs	$^4I_{9/2}$	18,919	10,293	23.56
	$^4I_{11/2}$	17,062	24,692	56.51
	$^4I_{13/2}$	15,083	4580.0	10.48
	$^4I_{15/2}$	13,023	341.93	0.78
	$^4F_{3/2}$	7549.9	428.65	0.98
	$^2H_{9/2}$	6867.9	2137.2	4.89
	$^4F_{5/2}$	6495.3	639.74	1.46
	$^4F_{7/2} + {}^4S_{3/2}$	5533.0	417.86	0.95
	$^4F_{9/2}$	4311.9	81.23	0.19
	$^2H_{11/2}$	3082.3	62.297	0.14
	$^4G_{5/2} + {}^2G_{7/2}$	1817.4	21.362	0.0005
			$\sum_{J'} A_{JJ'} = 43695$	
$^4G_{5/2} + {}^2G_{7/2}$ $\tau = 12$ μs	$^4I_{9/2}$	17,102	59,463	69.01
	$^4I_{11/2}$	15,244	21,345	24.77
	$^4I_{13/2}$	13,266	2495.6	02.90
	$^4I_{15/2}$	11,206	874.04	01.01
	$^4F_{3/2}$	5732.5	989.07	01.15
	$^2H_{9/2}$	5050.5	185.17	00.21
	$^4F_{5/2}$	4677.9	540.89	00.63
	$^4F_{7/2} + {}^4S_{3/2}$	3715.6	231.51	00.27
	$^4F_{9/2}$	2494.5	40.75	00.05
	$^2H_{11/2}$	1264.9	4.034	0.0
			$\sum_{J'} A_{JJ'} = 86169$	
$^2H_{11/2}$ $\tau = 794$ μs	$^4I_{9/2}$	15,837	169.25	13.43
	$^4I_{11/2}$	13,980	173.54	13.77
	$^4I_{13/2}$	12,001	123.87	09.83
	$^4I_{15/2}$	9940.6	710.00	56.35
	$^4F_{3/2}$	4467.6	2.4674	00.20
	$^2H_{9/2}$	3785.6	63.68	05.05
	$^4F_{5/2}$	3413.0	3.46	00.27
	$^4F_{7/2}$	2450.7	11.73	00.93
	$^4F_{9/2}$	1229.6	1.11	00.09
			$\sum_{J'} A_{JJ'} = 1260$	
$^4F_{9/2}$ $\tau = 95$ μs	$^4I_{9/2}$	14,607	751.49	07.15
	$^4I_{11/2}$	12,750	3524.4	33.53
	$^4I_{13/2}$	10,771	3701.1	35.21
	$^4I_{15/2}$	8711.0	2502.1	23.80
	$^4F_{3/2}$	3238.0	17.299	00.16
	$^2H_{9/2}$	2556.0	4.8326	00.05
	$^4F_{5/2}$	2183.4	7.2591	00.07
	$^4F_{7/2} + {}^4S_{3/2}$	1221.1	2.09	0.02

Table 4a (*Continued*)

Initial state and calculated radiative lifetime	Final state	ν (cm^{-1})	Radiative probability A (s^{-1})	Branching ratio β%
			$\sum_{J'} A_{JJ'} = 10511$	
$^4F_{7/2} + {}^4S_{3/2}$ τ = 38 μs	$^4I_{9/2}$	13,386	11,732	44.44
	$^4I_{11/2}$	11,529	7390.8	28.00
	$^4I_{13/2}$	9549.9	4178.9	15.83
	$^4I_{15/2}$	7489.9	3090.6	11.71
	$^4F_{3/2}$	2016.9	3.10	0.01
	$^2H_{9/2}$	1334.9	0.52	0.0
	$^4F_{5/2}$	962.30	0.90	0.0
			$\sum_{J'} A_{JJ'} = 26396$	
$^4F_{5/2}$ τ = 83 μs	$^4I_{9/2}$	12,424	7835.7	64.69
	$^4I_{11/2}$	10,567	1410.1	11.64
	$^4I_{13/2}$	8587.6	2415.8	19.95
	$^4I_{15/2}$	6527.6	448.90	3.71
	$^4F_{3/2}$	1054.6	1.16	0.0
	$^2H_{9/2}$	372.60	0.012	0.0
			$\sum_{J'} A_{JJ'} = 12112$	
$^4F_{3/2}$ τ = 107 μs	$^4I_{9/2}$	11,369	3668.2	39.25
	$^4I_{11/2}$	9512.0	4672.0	49.99
	$^4I_{13/2}$	7533.0	959.81	10.27
	$^4I_{15/2}$	5473.0	46.065	0.49
			$\sum_{J'} A_{JJ'} = 9346$	

Table 4b
Radiative parameters of Sm^{3+} doped ZnF_2–TeO_2 glasses mixed with 10 mol% of WO_3.

Initial state and calculated radiative lifetime	Final state	ν (cm^{-1})	Radiative probability A (s^{-1})	Branching ratio β%
$^4G_{5/2}$ τ = 2.2 ms	$^6H_{5/2}$	17,700	13.86	3.09
	$^6H_{7/2}$	16,669	238.02	53.13
	$^6H_{9/2}$	15,465	112.65	25.15
	$^6H_{11/2}$	14,142	59.65	13.31
	$^6H_{13/2}$	12,741	7.62	1.70
	$^6F_{1/2} + {}^6H_{15/2}$	11,269	0.76	0.06
	$^6F_{3/2}$	10,968	0.73	0.10
	$^6F_{5/2}$	10,491	8.22	0.16
	$^6F_{7/2}$	9657.0	4.8100	1.83
	$^6F_{9/2}$	8505.0	1.25	1.07
	$^6F_{11/2}$	7159	0.44	0.28
			$\sum_{J'} A_{JJ'} = 448$	

ation i.e., the transfer of energy from the excited state of Sm-ion by electric multipole interaction (more precisely dipole-dipole or dipole-quadrapole interactions) to neighboring Sm-ion lying in the ground state is low for this particular glass when compared with other glasses of this system. In the emission spectra, the transition $^4G_{5/2} \rightarrow {}^6H_{7/2}$ with $\Delta J = \pm 1$ is a magnetic dipole (MD) allowed where as the transition $^4G_{5/2} \rightarrow {}^6H_{9/2}$ is purely electric dipole one. The intensity ratio of electric dipole to magnetic dipole transitions is a measure of the asymmetry of the local environment of Sm^{3+} ions. The greater the intensity ratio of the electric dipole transition to the magnetic dipole transition ($I_{4G5/2 \rightarrow 6H9/2}/I_{4G5/2 \rightarrow 6H7/2}$) the more is the asymmetry of Sm^{3+} in the network [23]. In the present work, this ratio is evidently more for the glass SmW_{15} indicating the highest local disorder for the Sm^{3+} ion in the network of this glass.

The absorption and emission spectra of Eu^{3+} show special characteristics not exhibited by the other rare earth ions. The relative emission intensities of transitions occurring in the low-energy region to those in the high-energy region are quite sensitive to the host matrix. Hypersensitive transitions invariably appear, as intense emission bands in the low-energy region and are influenced by micro-symmetry under-covalency of the rare earth ions. Further, the transition $^5D_0 \rightarrow {}^7F_0$ in the emission spectra is typical for coordination of the Eu^{3+} ion. This transition observed at about 17,200 cm^{-1} for the studied glasses suggests 8–9 coordination for Eu^{3+} ion in the glass network [65]. This transition is purely electric dipole in nature and can therefore be expected to give reliable values for the radiative parameters unlike other transitions which arise due to J mixing or pure magnetic dipole transitions. The tran-

Table 4c
Radiative parameters of Eu^{3+} doped ZnF_2–TeO_2 glasses mixed with 10 mol% of WO_3.

Initial state and calculated radiative lifetime	Final state	ν (cm^{-1})	Radiative probability A (s^{-1})	Branching ratio β%
$^5D_0$ τ = 2.9 ms	$^7F_1$	16,806.7	49	14.5
	$^7F_2$	16,233.8	251	73.7
	$^7F_4$	14,204.6	40	11.8
			$\sum_{J'} A_{JJ'} = 340$	

Table 5
A comparison of radiative lifetimes (τ) and quantum efficiencies (η) for the principal transitions in ZnF_2–WO_3–TeO_2:Ln^{3+} glasses.

WO_3 conc. (mol%)	Nd^{3+} doped glasses ($^4F_{3/2}$ level)			Sm^{3+} doped glasses ($^4G_{5/2}$ level)			Eu^{3+} doped glasses ($^5D_0$ level)		
	τ_m (μs)	τ_c (μs)	η%	τ_m (ms)	τ (ms)	η%	τ_m (ms)	τ (ms)	η%
5	65.14	95	68.57	0.98	1.60	61.25	1.04	2.50	41.60
10	82.52	107	77.12	1.48	2.20	67.27	1.27	2.90	43.79
15	102.06	116	87.98	1.93	2.72	70.96	1.69	3.25	52.0
20	91.20	109	83.67	1.80	2.61	68.97	1.39	2.85	48.77

sitions $^5D_0 \rightarrow {}^7F_2$ and $^5D_0 \rightarrow {}^7F_1$ occur in the red (R) and orange (O) regions, respectively and intensities of these transitions depend on the Judd–Ofelt parameters Ω_2 and Ω_4 or in other words the integrated emission intensity ratio of these two transitions (R/O ratio) is strongly influenced by site asymmetry (or structural changes in the vicinity of the Eu^{3+} ion) and covalency of the bonds with the ligand anions [65,66]. The values of this ratio shows a decreasing trend (EuW_5 = 5.32, EuW_{10} = 5.19, EuW_{15} = 4.92 and EuW_{20} = 5.16) with the increase in the concentration of WO_3 up to 15 mol%, indicating decreasing covalent environment for Eu^{3+} ions in this concentration range of WO_3.

The parameter β_r (i.e., the branching ratio) of the luminescence transitions characterizes the lasing power of the potential laser transitions. The β_r values obtained for various luminescent transitions for the three rare earth ions of the glasses mixed with 10 mol% of WO_3 are furnished in Table 3a–c. It was well established that an emission level with β_r value nearly equal to 50% is a potential laser emission [67]. Among various transitions, the transitions $^4F_{3/2} \rightarrow {}^4I_{11/2}$, $^4G_{5/2} \rightarrow {}^6H_{7/2}$, $^5D_0 \rightarrow {}^7F_2$ respectively for Nd^{3+}, Sm^{3+} and Eu^{3+} doped glasses found to have the highest values of β_r for all the three glasses; these transitions may therefore be considered as a possible laser transitions. Further, the comparison of β_r values of these transitions for the glasses mixed with different concentrations of WO_3 shows the largest value for LnW_{15} glasses indicating that these glasses exhibit better lasing action (Table 5).

The fluorescence decay curves of the emission lines corresponding to $^4F_{3/2}$, $^4G_{5/2}$, $^5D_0$ levels of Nd^{3+}, Sm^{3+} and Eu^{3+} ions respectively in ZnF_2–TeO_2 glasses mixed with different concentrations of WO_3 are recorded at room temperature and the log of intensity dependences with the decay time are shown in Fig. 11; the variation indicates that the decay is single exponential. The fluorescence lifetime τ, evaluated from these graphs is apparently shorter than calculated life times from the J–O theory (Table 5). Such difference may indicate on multi-phonon relaxations. The increasing trend of life time either calculated or measured for the glasses LnW_5 to LnW_{15} suggests a decreasing trend of phonon loses or increasing presence of W^{5+} ions that act as modifier in these glasses.

Normally, the non-radiative processes, the total radiative lifetime τ_m of particular level is defined as

$$\frac{1}{\tau_m} = A_{rad} + W_{mp} \tag{6}$$

where A_{rad} is the radiative decay rate (in the absence of non-radiative losses) and W_{mp} represents the multi-phonon decay rate of Ln^{3+} ions given by

$$W_{mp}(T) = W_0 \left[\frac{\exp(\hbar\omega/kT)}{\exp(\hbar\omega/kT) - 1} \right]^p \tag{7}$$

where $W_0 = W_{mp}$ (T = 0 K) = $C\exp(-\alpha\Delta E)$.

ΔE is represents the gap between the levels of interest and p is the number of phonons given $\Delta E/\hbar\omega$. Additionally, some aggregations and interaction with the phonon subsystem may also be responsible for the observed variations in the radiative decay rate for these samples. Thus following the radiative life times, it is evident that there is a gradual decrease of interaction of Ln^{3+} ions with the glass network in the glasses from LnW_5 to LnW_{15} since τ_m is observed to increase with increase in the concentration of WO_3 up to 15 mol%.

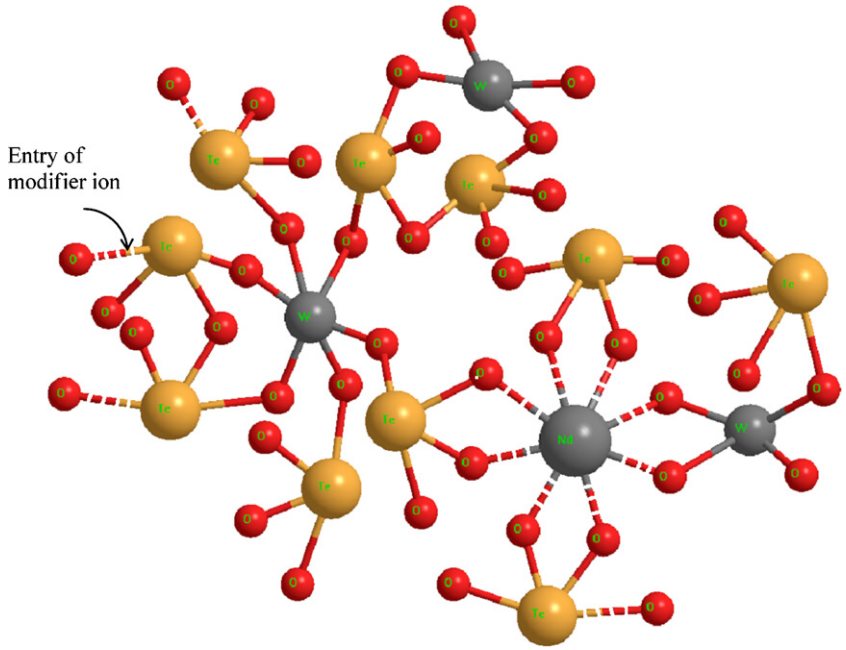

Fig. 10. An illustration of Nd^{3+} ion embedded in TeO_2 glass network with tungsten ions in tetrahedral and octahedral positions.

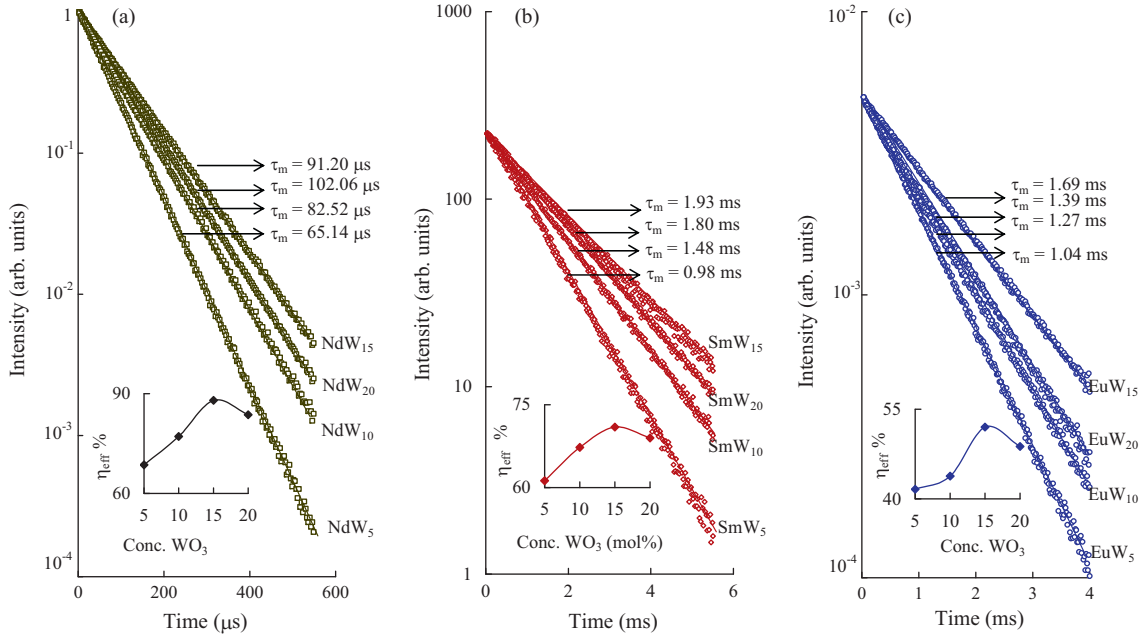

Fig. 11. The variation of fluorescence intensity with the time of the emission lines of (a) $^4F_{3/2}$ (Nd^{3+}), (b) $^4G_{5/2}$ (Sm^{3+}), and (c) $^5D_0$ (Eu^{3+}) levels respectively in ZnF_2–TeO_2 glasses mixed with different concentrations of WO_3. Insets represent the variation of luminescence efficiency with the concentration of WO_3.

The quantum yield (η) is defined as the radiative portion of the total relaxation rate of a given energy level [68]:

$$\eta = \frac{A_{rad}}{A_{rad} + W_{nr}} = \frac{\tau_{exp}}{\tau_{rad}} \quad (8)$$

where A_{rad} is the total radiative relaxation rate, W_{nr} is the rate of total non-radiative transition τ_{exp} – experimental lifetime, τ_{rad} – radiative lifetime. The value of η for the three principal levels viz., $^4F_{3/2}$, $^4G_{5/2}$, $^5D_0$ of Nd^{3+}, Sm^{3+} and Eu^{3+} ions respectively are determined and presented in Table 4. As the concentration of WO_3 is increased from 5 to 15 mol%, the value of η is observed to increase considerably; such rise is connected not only with the rise of the radiative relaxation probability but also with a reduction of the non-radiative transition probability. This is possibly due to the decrease of the electron–phonon coupling of the Ln^{3+} ion with the high-energy phonons and relative increase of this coupling with low-energy phonons in the TeO_2 glass network [69].

The radiative transition probabilities for all the three rare earth doped glasses mixed with 20 mol% of WO_3 show a deviation from those of the glasses LnW_5, LnW_{10}, LnW_{15}; such trend suggests that the reduction of tungsten ions to W^{5+} state is considerably less in this glass. Major proportion exists in W^{6+} states and participate in the glass network (this is also evidenced from IR, Raman and ESR spectral studies) causing to lower values of transition probabilities.

5. Conclusions

Glasses of the composition $(45-x)ZnF_2$–xWO_3–$49TeO_2$: $1.0Nd_2O_3/Sm_2O_3/Eu_2O_3$ with x varying from 5 to 20 mol% have been prepared. DSC, IR, Raman, ESR, optical absorption and photoluminescence studies have been carried out. ESR studies have indicated that the tungsten ions exist in W^{5+} state, in addition to W^{6+} state. IR and Raman spectral studies have suggested that there is a growing degree of disorder in the glass network with increase in the concentration of WO_3 up to 15 mol%. The Judd–Ofelt theory could successfully be applied to characterize the optical absorption spectra of three rare earth ions; out of the three J–O parameters (Ω_λ), the value of Ω_2, which is related to the structural changes in the vicinity of the Ln^{3+} ion exhibited a gradual decrease with increase in the concentration of WO_3 up to 15 mol%. From this observation it is concluded that there is gradual increase in the degree of disorder or asymmetry in the glass network. The radiative transition probabilities and branching ratios evaluated for various luminescent transitions observed in the luminescence spectra, suggested the highest values for $^4F_{3/2} \rightarrow {}^4I_{11/2}$ (Nd^{3+}), $^4G_{5/2} \rightarrow {}^6H_{7/2}$ (Sm^{3+}) and $^5D_0 \rightarrow {}^7F_2$ (Eu^{3+}). The comparison of β_r values of these transitions showed the largest value for glass mixed with 15 mol% of WO_3. Finally, with the aid of the data on ESR, IR and Raman spectral studies, it is concluded that the glass containing the highest concentration of tungsten ions in W^{5+} state is preferable for achieving the highest luminescence efficiency for all the three rare earth ions.

References

[1] I. Ardelean, S. Lupsor, D. Rusu, Physica B 405 (2010) 2259.
[2] T. Hayakawa, M. Hayakawa, M. Nogami, P. Thomas, Opt. Mater. 32 (2010) 448.
[3] D.K. Durga, N. Veeraiah, J. Mater. Sci. 36 (2001) 5625.
[4] Y. Gandhi, N. Venkatramaiah, V. Ravikumar, N. Veeraiah, Physica B 404 (2009) 1450.
[5] F. Chen, T. Xu, S. Dai, Q. Nie, X. Shen, J. Zhang, X. Wang, Opt. Mater. 32 (2010) 868.
[6] J. Ozdanova, H. Ticha, L. Tichy, Opt. Mater. 32 (2010) 950.
[7] C. Laxmikanth, B.V. Raghavaiah, B. Appa Rao, N. Veeraiah, J. Lumin. 109 (2004) 193.
[8] I. Jlassi, H. Elhouichet, M. Ferid, R. Chtourou, M. Oueslati, Opt. Mater. 32 (2010) 743.
[9] G. Poirier, F.C. Cassanjes, Y. Messaddeq, S.J.L. Ribeiro, J. Non-Cryst. Solids 355 (2009) 441.
[10] C. Lasbrugnas, P. Thomas, O. Masson, J.C. Champarnaud-Mesjard, E. Fargin, V. Rodriguez, M. Lahaye, Opt. Mater. 31 (2009) 775.
[11] P. Subbalakshmi, N. Veeraiah, J. Non-Cryst. Solids 298 (2002) 89.
[12] Y. Gandhi, K.S.V. Sudhakar, M. Nagarjuna, N. Veeraiah, J. Alloys Compd. 485 (2009) 876.
[13] Y.B. Saddeek, Philos. Mag. 89 (2009) 41.
[14] A. Sheoran, S. Sanghi, S. Rani, A. Agarwal, V.P. Seth, J. Alloys Compd. 475 (2009) 804.
[15] U. Hoppe, E. Yousef, C. Rüssel, J. Neuefeind, A.C. Hannon, J. Phys. Condens. Matter 16 (2004) 1645.
[16] G. Liao, Q. Chen, J. Xing, H. Gebavi, D. Milanese, M. Fokine, M. Ferraris, J. Non-Cryst. Solids 355 (2009) 447.
[17] P. Chimalawong, J. Kaewkhao, C. Kedkaew, P. Limsuwan, J. Phys. Chem. Solids 71 (2010) 965.
[18] J.W. Pisarska, A. Pisarski, W. Ryba-Romanowski, Opt. Laser Technol. 42 (2010) 805.

[19] K.B. Yatsimirskii, N.K. Davidenko, Coord. Chem. Rev. 27 (1979) 223.
[20] L. Srinivasa Rao, M. Srinivasa Reddy, M.V. Ramana Reddy, N. Veeraiah, Physica B 403 (2008) 2542.
[21] R. Reisfeld, C.K. Jorgensen, Lasers and Excited states of Rare Earths, Springer-Verlag, New York, 1977.
[22] K. Hairao, S. Todoroki, D.H. Cho, N. Soga, Opt. Lett. 18 (1993) 1586.
[23] A. Kurita, T. Kushida, T. Izumitani, M. Matsukawa, Opt. Lett. 19 (1994) 314.
[24] K.K. Mahato, D.K. Rai, S.B. Rai, Solid State Commun. 108 (1998) 671.
[25] J. Zhang, D.L. Yang, E.Y.B. Pun, H. Gong, H. Lin, J. Appl. Phys. 107 (2010) 123111.
[26] K.S.V. Sudhakar, M. Srinivasa Reddy, L. Srinivasa Rao, N. Veeraiah, J. Lumin. 128 (2008) 1791.
[27] Z. Mazurak, S. Bodył, R. Lisiecki, J. Gabryś-Pisarska, M. Czaja, Opt. Mater. 32 (2010) 547.
[28] G. Lakshminarayana, R. Yang, M. Mao, J. Qiu, I.V. Kityk, J. Non-Cryst. Solids 355 (2009) 2668.
[29] R. Reisfeld, Structure and Bonding 22, Springer-Verlag, New York, 1975.
[30] D.E. Henrie, R.L. Fellows, G.R. Choppin, Coord. Chem. Rev. 18 (1976) 199.
[31] W.D. Horrocks Jr., M. Albin, Prog. Inorg. Chem. 31 (1984) 1 (An Interscience Publication, New York).
[32] K. Hirao, S. Todoroki, N. Soga, J. Non-Cryst. Solids 175 (1994) 263.
[33] G. Boulon, M. Bouderbala, J. Seriot, J. Less-Common Met. 112 (1985) 41.
[34] M. Nogami, A. Ohno, H. You, Phys. Rev. B 68 (2003) 104204.
[35] C. Shen, S. Baccaro, Z. Xing, Q. Yan, S. Wang, G. Chen, Chem. Phys. Lett. 492 (2010) 123.
[36] V. Ravikumar, N. Veeraiah, B. Appa Rao, J. Mater. Sci. 33 (1998) 2659.
[37] J. Ozdanova, H. Ticha, L. Tichy, J. Non-Cryst. Solids 355 (2009) 2318.
[38] D. Munoz-Martín, M.A. Villegas, J. Gonzalo, J.M. Fernández-Navarro, J. Eur. Ceram. Soc. 29 (2009) 2903.
[39] Y. Gandhi, M.V. Ramachandra Rao, Ch. Srinvasa Rao, T. Srikumar, I.V. Kityk, N. Veeraiah, J. Appl. Phys. 108 (2010) 023102.
[40] T. Satyanarayana, M.G. Brik, N. Venkatramaiah, I.V. Kityk, K.J. Plucinski, V. Ravikumar, N. Veeraiah, J. Am. Ceram. Soc. 93 (2010) 2004.
[41] I. Morozova, A. Yakind, Fis. Khim. Stekla 3 (1977) 197.
[42] K.J. Rao, Structural Chemistry of Glasses, Elsevier, Amsterdam, 2002.
[43] G. Upender, C.P. Vardhani, S. Suresh, A.M. Awasthi, V. Chandra Mouli, Mater. Chem. Phys. 121 (2010) 335.
[44] Z. Pan, D.O. Henderson, S.H. Morgan, J. Non-Cryst. Solids 171 (1994) 134.
[45] T. Sekiya, N. Mochida, A. Ohtsuka, T. Tonokawa, J. Non-Cryst. Solids 144 (1992) 128.
[46] H. Burger, K. Kneipp, H. Hobert, J. Non-Cryst. Solids 151 (1992) 134.
[47] B.V.R. Chowdari, P. Pramoda Kumari, Solid State Ionics 113 (1998) 665.
[48] A. Goldstein, V. Chiriac, D. Becherescu, J. Non-Cryst. Solids 92 (1987) 271.
[49] P. Subbalakshmi, B.V. Raghavaiah, R. Balaji Rao, N. Veeraiah, EPJ Appl. Phys. 26 (2004) 169.
[50] B.R. Judd, Phys. Rev. 127 (1962) 750.
[51] G.S. Ofelt, J. Chem. Phys. 37 (1962) 511.
[52] B.M. Walsh, Judd-Ofelt theory: principles and practices, in: B. Di Bartolo, O. Forte (Eds.), Advances in Spectroscopy for Lasers and Sensing, Springer, The Netherlands, 2006, pp. 403–433.
[53] C.K. Jorgenson, Orbitals Atoms and Molecules, Academic Press, London, 1962.
[54] S.P. Sinha, Complexes of the Rare Earths, Pergamon, Oxford, 1966.
[55] N. Mochida, K. Takahashi, K. Nakata, Yogyo Kyokai Shi 86 (1978) 316.
[56] V. Dimitrov, M. Arnaudov, Y. Dimitriev, Monatsh. Chem. Chem. Monatsh. 115 (1984) 987.
[57] K. Sambasiva Rao, M. Srinivasa Reddy, V. Ravi Kumar, N. Veeraiah, Mater. Chem. Phys. 111 (2008) 283.
[58] S. Muthupari, S. Prabakar, K.J. Rao, J. Phys. Chem. Solids 57 (1996) 553.
[59] A. Brenier, I.V. Kityk, J. Appl. Phys. 90 (2001) 232.
[60] S.M.D. Nery, W.M. Pontuschka, S. Isotani, C.G. Rouse, Phys. Rev. B 49 (1994) 3760.
[61] J. Lucas, J. Less-Common Met. 112 (1985) 27.
[62] H. Ahrens, M. Wollenhaupt, P. Frobel, J. Lin, K. Barner, G.S. Sun, R. Braunstein, J. Lumin. 82 (1999) 177.
[63] A.G.S. Filho, J.M. Filho, F.E.A. Melo, M.C.C. Custodio, R. Lebullenger, A.C. Hernandes, J. Phys. Chem. Solids 61 (2000) 1535.
[64] K. Devlin, B. O' Kelly, Z.R. Tang, C.Mc. Donagh, J.F.Mc. Glip, J. Non-Cryst. Solids 135 (1991) 8.
[65] Q. Su, Z. Pei, L. Chi, H. Zhang, Z. Zhang, F. Zou, J. Alloys Compd. 192 (1993) 25.
[66] E.W.J.L. Oomen, A.M.A. va Dongen, J. Non-Cryst. Solids 111 (1989) 205.
[67] C. Hirayama, F.E. Camp, N.T. Melamid, K.B. Steinbruegge, J. Non-Cryst. Solids 6 (1971) 342.
[68] M. Rozanski, K. Wisniewski, J. Szatkowski, Cz. Koepke, M. Sroda, Opt. Mater. 31 (2009) 548.
[69] R. Lam, T. Langet, J.E. Greedan, J. Solid State Chem. 171 (2003) 317.